Mon. Not. R. Astron. Soc. **278**, 345–366 (1996)

# A stellar and gas dynamical numerical model of ring galaxies

R. A. Gerber,[1,2,3] S. A. Lamb[2,3] and D. S. Balsara[3,4]

[1]*Present address: Space Science Divison, NASA Ames Research Center, Mail Stop 245-3, Moffett Field, CA 94035, USA*
[2]*Department of Physics, University of Illinois, Urbana, IL 61801, USA*
[3]*Department of Astronomy, University of Illinois, Urbana, IL 61801, USA*
[4]*Present address: National Center for Supercomputing Applications, University of Illinois, Urbana, IL 61801, USA*

Accepted 1995 July 11. Received 1995 June 5; in original form 1994 September 5

**ABSTRACT**

The formation and evolution of ring galaxies, produced by collisions between two galaxies, are investigated using a three-dimensional, combined N-body/hydrodynamical computer code. Specifically, the dependence of ring structure and temporal development is studied as a function of the mass ratio between the two colliding galaxies: a gas-rich disc galaxy and a gas-free spherical galaxy. The morphology, density, and velocity structures are given for both the stellar and gaseous components of the disc.

A collision between two galaxies of equal mass is shown to be qualitatively different in many respects when compared with a collision involving galaxies of unequal mass.

**Key words:** hydrodynamics – galaxies: interactions – galaxies: kinematics and dynamics.

## 1 INTRODUCTION

Ring galaxies are the product of perhaps the simplest of galactic collisions involving a disc galaxy. When one galaxy strikes another's disc at normal incidence near its centre, the disc responds by forming an expanding ring. A complete understanding of such symmetric systems is important for the study of the usual phenomena associated with interacting galaxies.

In particular, large-scale bursts of star formation are observed in many ring galaxies, as is also the case for colliding galaxies in general. In contrast to many interacting systems, which often show signs of unusually active star formation in their nuclei, the vigorous star formation in ring galaxies is located in the extranuclear ring. Thus it is observationally easier to separate indicators of star formation from those of other interaction-induced processes, such as gas accretion on to a central black hole. The star formation in the ring is coherent on the scale of kiloparsecs and is observed in a number of systems (e.g., Theys & Spiegel 1976; Fosbury & Hawarden 1977; Thompson & Theys 1978; Jeske 1986; Appleton & Struck-Marcell 1987b; Gerber, Lamb & Balsara 1992; Marcum, Appleton & Higdon 1992; Higdon 1993; Mihos & Hernquist 1994).

As a basis for future modelling and in an effort to understand the character of large-scale flows of both stars and the gaseous interstellar medium in ring galaxies, we have carried out a limited number of numerical calculations which follow the formation and subsequent evolution of interacting ring galaxies.

Our goal is to understand the connection between galaxy collisions and induced star formation; however the mechanism by which star formation is triggered in these systems is poorly understood. Qualitatively, it is plausible that any or all of the following processes take place and contribute to the star formation process: (1) shocks initiate the formation of dense, gravitationally unstable clouds, which form from a more rarefied interstellar medium (ISM); (2) the passage of a shock front increases the surface pressure on pre-existing non-critical clouds, triggering their collapse; and (3) cloud–cloud collisions and mergers lead to star formation.

Whatever the mechanism, stars form from the ISM and the first step toward understanding the nature of the triggered star formation is to study the large-scale dynamics of a simplified model of the gas in a spiral galaxy. We represent the ISM as a continuous single-component medium, here ignoring its multi-component structure, which may include dense clouds embedded in a diffuse background.

Ring galaxies are excellent laboratories for this study. Their simple, almost axially symmetric, geometry facilitates modelling of the two-galaxy orbital parameters. Ring galaxies are produced by the collision of two galaxies, providing that at least one was originally a disc galaxy. When one galaxy strikes the other's disc at near normal incidence and near its centre, disc material is gathered into an expanding ring. Theoretical studies have shown that ring formation is the natural outcome of such a collision (Lynds & Toomre 1976; Toomre 1978; Appleton & Struck-Marcell 1987a; Huang & Stewart 1988; Struck-Marcell 1990; Struck-Marcell & Lotan 1990; Gerber 1993; Struck-Marcell & Higdon 1993; Hernquist & Weil 1993; Gerber & Lamb 1994). Observationally, Theys & Spiegel (1976) found that bright ring galaxies in their sample have nearby galaxies aligned with the apparent minor axis of the rings (see also Few & Madore 1986).

In this paper we investigate computationally the collision of a disc galaxy containing a centrifugally supported disc of both gas and stars with a gas-free spherical galaxy (the 'intruder'). The spherical galaxy passes through the centre of the disc galaxy, along the disc's axis of rotation. Three collisions are considered in which the disc galaxy to intruder mass ratios are 1:1, 4:1 and 10:1. The numerical code is a combined three-dimensional N-body, smoothed particle hydrodynamics (SPH) code with a resolution which scales to approximately 800 pc – 1 kpc in a disc galaxy comparable to the Milky Way.

Previous studies of induced star formation in interacting galaxies have modelled the star formation process in various manners. Many have assumed that collisions between individual gas clouds are important in the production of new stars (e.g., Olson & Kwan 1990a, 1990b; Scalo & Struck-Marcell 1986; Noguchi & Ishibashi 1986; Lattanzio et al. 1986). In these simulations, neighbouring clouds are assumed to interact in a parametrized way that produces dissipation. In addition gas may be turned into stars in some prescribed manner and further parameters can control the amount of gas depletion and energy feedback into the ISM.

The primary drawback to these studies is that the physics of interstellar cloud collisions is largely unknown and the outcome of cloud–cloud collisions is uncertain. Further, any role cloud collisions may have on the triggering of star formation is not known.

Jog & Solomon (1992) and Jog & Das (1992) use a criterion for star formation whereby a hot intercloud medium supplies an overpressure on clouds, which leads to their collapse. Jog & Solomon's contention that stars only form in the overlap regions between two gas-rich disc galaxies seems too conservative, though. It is shown in Gerber et al. (1992) that shocks and compressions can form in the ISM of a disc galaxy if it is impacted by a gas-free companion. Mihos & Hernquist (1994) introduced an algorithm for star formation which is based on the Schmidt law (Schmidt 1959), a relationship which has been calibrated for 'normal' spiral galaxies, in which the star formation rate is assumed to be proportional to the local gas density.

In this paper we do not explicitly model the star formation process, focusing instead on the behaviour of large-scale flows of both stars and gas, and the resulting difference in the structure of these two components. However, as a motivation for this study, we suggest that one likely trigger for producing bursts of high-mass extranuclear star formation is compressions and shocks that form in a continuous background interstellar medium. Shocks can implode pre-existing clouds and provide a perturbation to initiate the formation of large cloud complexes via the magnetic Rayleigh–Taylor, or Parker, instability. A mechanism describing this scenario was proposed by Mouschovias, Shu & Woodward (1974) in the context of star formation due to the passage of a spiral arm shock (see also Roberts 1969). It offers an explanation of the observed spacing of large star forming regions in the spiral arms of external galaxies, often described as 'beads on a string' (see also Woodward 1976). A similar structure is seen in collisionally produced ring galaxies (e.g., Theys & Spiegel 1976; Higdon 1993), in which a strong circular density wave is expanding in the disc (Lynds & Toomre 1976).

In this paper we determine the location of shock fronts and large-scale density enhancements and argue that these are likely regions of active star formation.

The remainder of this paper is divided into four sections. In Section 2 we describe our numerical methods and model galaxies. Our results are presented in Section 3, and we discuss the possible implications of the results in Section 4. Section 5 contains a summary of our findings.

## 2 THE MODEL AND NUMERICAL METHODS

A summary of the numerical methods and the initial galaxy models are given below. Details can be found in the appendix to this paper, in Balsara (1990) and in Gerber (1993).

### 2.1 Numerical methods

The gas dynamics is modelled numerically using the method of smoothed particle hydrodynamics (SPH) (e.g., Lucy 1977; Gingold & Monaghan 1982; Hernquist & Katz 1989; Balsara 1990; Monaghan 1992). In SPH, particles are used to represent the gas continuum. The density is obtained by smoothing out the mass of nearby particles using an analytic smoothing kernel and forces are calculated by taking gradients of a smoothed estimate of the pressure. Balsara's (Balsara 1990) artificial viscosity formulation is used to capture shock behaviour. We use an ideal gas equation of state and fluid elements are forced to remain at a constant temperature throughout the simulations.

The gravitational force is calculated using standard particle-mesh (PM) techniques (see Hockney & Eastwood 1988). The gravitational potential is calculated at a restricted number of points on a three-dimensional grid and the force on an individual particle is determined by interpolation between grid points. Both the stellar and SPH particles contribute to the gravitational potential. In the experiments described in this paper we use a cubic grid with 64 points along each side, approximately 60 000 N-body particles, and 22 500 SPH particles. More details of the combined code can be found in Balsara (1990), where tests of it are presented.

Computations were conducted on the Cray YMP and Cray-2 supercomputers at the National Center for Supercomputing Applications at the University of Illinois at Urbana-Champaign and on the Cray YMP C90 at the Numerical Aerodynamics Simulation facility at NASA Ames Research Center.

### 2.2 Model galaxies

The model 'spiral' galaxy contained a disc with a stellar and gaseous surface density that declined exponentially with radius, surrounded by a massive, almost spherical halo of particles. The elliptical galaxy was represented by a spherical distribution of stars only. All particles were 'live', that is they contributed to the gravitational potential and were free to respond to gravitational forces.

The stellar disc with surrounding halo was similar to that described in Barnes (1988) and is described in more detail in the appendix to this paper and in Gerber (1993). The halo had 24 953 particles, the disc consisted of 25 000 particles in rotation around the centre and Toomre's stability parameter, $Q$ (Toomre 1964), was set to 1.5 everywhere in the disc. In cylindrical coordinates $(r, z)$, the three-dimensional

density distribution, $\rho$, of the disc was

$$\rho(r,z) = \frac{M_{\rm exp}}{4\pi H R_{\rm d}^2} \exp(-\frac{r}{R_{\rm d}}) \,{\rm sech}^2(\frac{z}{H})$$

where the scale height, $H$, was set constant with radius, and $M_{\rm exp}$ was the total mass of a radially infinite exponential disc with disc radial scale length $R_{\rm d}$. The disc density distribution was cut off at $4.4\,R_{\rm d}$; interior to which radius the integrated mass was $0.93 M_{\rm exp}$. Perpendicular to the disc the density distribution of the disc was cut off after two scale heights, where the density was 0.07 of its midplane value.

Approximately 22 500 SPH particles were used to model the gaseous disc. The gas density distribution followed that of the disc stars with a total mass equal to one tenth that of the stellar disc. The SPH particles were placed in circular orbits around the centre of the galaxy.

The gas-free elliptical galaxy was represented by a spherical King model with 10 000 N-body particles. Three separate runs were performed in which the ratio of disc galaxy to intruder mass was 1:1, 4:1 and 10:1. The ratio of disc cutoff radius to intruder radius was approximately 1:1, 2:1 and 3:1. The spherical mass distributions of both galaxies were meant to model both the stellar component and a 'dark matter' halo. The initial relative speed of the two centres of mass was chosen to give a mildly hyperbolic orbit. The initial centre of mass separation of the two galaxies was about 7 radial disc scale lengths at the start of the experiment.

As a test of their stability, the models were evolved in isolation for a period longer than the duration of the collision experiments. The disc exhibited a tendency to produce low-amplitude spiral patterns and expanded slightly in the direction normal to the plane, but no large-scale changes in the galaxies occurred (see Gerber 1993).

### 2.3 Scaling

For purposes of discussion in the later sections of the paper we have scaled numerical parameters so that the disc galaxy represents a galaxy similar to the Milky Way. With this choice the disc has a total mass of $5 \times 10^{10}\,{\rm M}_\odot$, the total gas mass is $5 \times 10^{9}\,{\rm M}_\odot$, and the halo mass is $1.25 \times 10^{11}\,{\rm M}_\odot$. The disc scale radius, $R_{\rm d}$, is 4 kpc and the disc is cut off at a radius of 17.6 kpc. The disc rotation velocity, averaged over the entire disc, is 211 km s$^{-1}$. The scale height in the direction perpendicular to the disc is 800 pc. The gas density ranges from about 0.002 cm$^{-3}$ above the outer edge of the disc to about 0.7 cm$^{-3}$ at the centre of the disc. The intruder masses are $1.75 \times 10^{11}\,{\rm M}_\odot$, $4.375 \times 10^{10}\,{\rm M}_\odot$, and $1.75 \times 10^{10}\,{\rm M}_\odot$. The relative velocity of approach of the two galaxies' centres of mass is 455 km s$^{-1}$ at an initial separation of 30 kpc.

## 3 RESULTS

Presentation of our results is divided into sections: the first contains a morphological description of the collision; density and velocity fields are given in subsequent sections. For brevity, the collision between equal-mass galaxies will be denoted as experiment C-1, the 4:1 mass-ratio experiment will be referred to as experiment C-4, and the 10:1 mass-ratio run is C-10.

### 3.1 Morphology

A time sequence showing the intruder and the edge-on stellar disc for the equal-mass collision C-1 is presented in Fig. 1. Time in all the figures is given relative to the time when the two galaxies' centres of mass coincide. Corresponding views for experiments C-4 and C-10 are not shown, but are similar except that the disc remains planar to a greater extent than in experiment C-1. The disc, viewed from above, is shown in Figs 2–7, for the three experiments. Some care should be taken when viewing plots of SPH particle position; while the plots do indicate the morphology, the particles have differing masses and a high density of SPH particles do not necessarily indicate a proportionally high gas density.

The collisionless particles respond similarly to those in previous investigations (e.g., Lynds & Toomre 1976; Huang & Stewart 1988; Theys & Spiegel 1977). The disc initially contracts radially and bows toward the incoming intruder. Soon after close approach, the inflow produces a density enhancement in the inner parts of the galaxy. The inward motion stops when the particles reach their centrifugal barrier and 'bounce' outward. The particles in the inner part of the disc start moving outward first, while the outer parts of the disc are still contracting.

The qualitative behaviour of the particles can be understood if one regards the stars as executing radial oscillations about their initial circular orbits after receiving a radial velocity perturbation from the intruder. The frequency of these epicyclic oscillations decreases with increasing radial position; the different time-scales in different parts of the disc cause stellar orbits to crowd together and perhaps cross, forming a density wave pattern that propagates outwards as an expanding ring (see Lynds & Toomre 1976; Struck-Marcell & Lotan 1990). This picture breaks down in detail in a collision of equal-mass galaxies. In experiment C-1, for example, there is bulk motion of material (both stars and gas) over distances large compared with the initial disc dimension.

The time-scale for ring formation and expansion increases with increasing mass ratio between the two galaxies. In experiment C-1, the ring moves outward through the disc quickly; compared with the rings in experiments C-4 and C-10, the lifetime of the C-1 ring is brief. By 100 Myr the stellar ring has largely dispersed. A large amount of the disc material is contained in the C-1 ring and the disc surface density has changed from a smooth exponential to a diffuse structure with a relatively dominant nucleus (140 Myr) and a radial extent much greater than that of the initial disc.

The rings in experiments C-4 and C-10 behave quite differently. The C-4 ring expands faster than the C-10 ring, but in both cases the ring is much more of a 'wave' phenomenon, as opposed to the large-scale bulk motion of material that occurs in experiment C-1. By 140 Myr , the C-4 ring has not yet reached the edge of the original disc. An inner ring of star particles is difficult to discern in particle plots of experiment C-1 (although it can be seen in the surface density plot of Fig. 8), but is obvious in experiments C-4 and C-10. This inner ring forms at the same radius at the same time in all three experiments, but the location of the outer ring is sensitive to the mass ratio, suggesting that the ratio of outer to inner ring radius contains information about the mass ratio between the host and intruder galaxies (see Stuck-Marcell & Lotan 1990).

The gaseous ring always has much sharper, thinner fea-

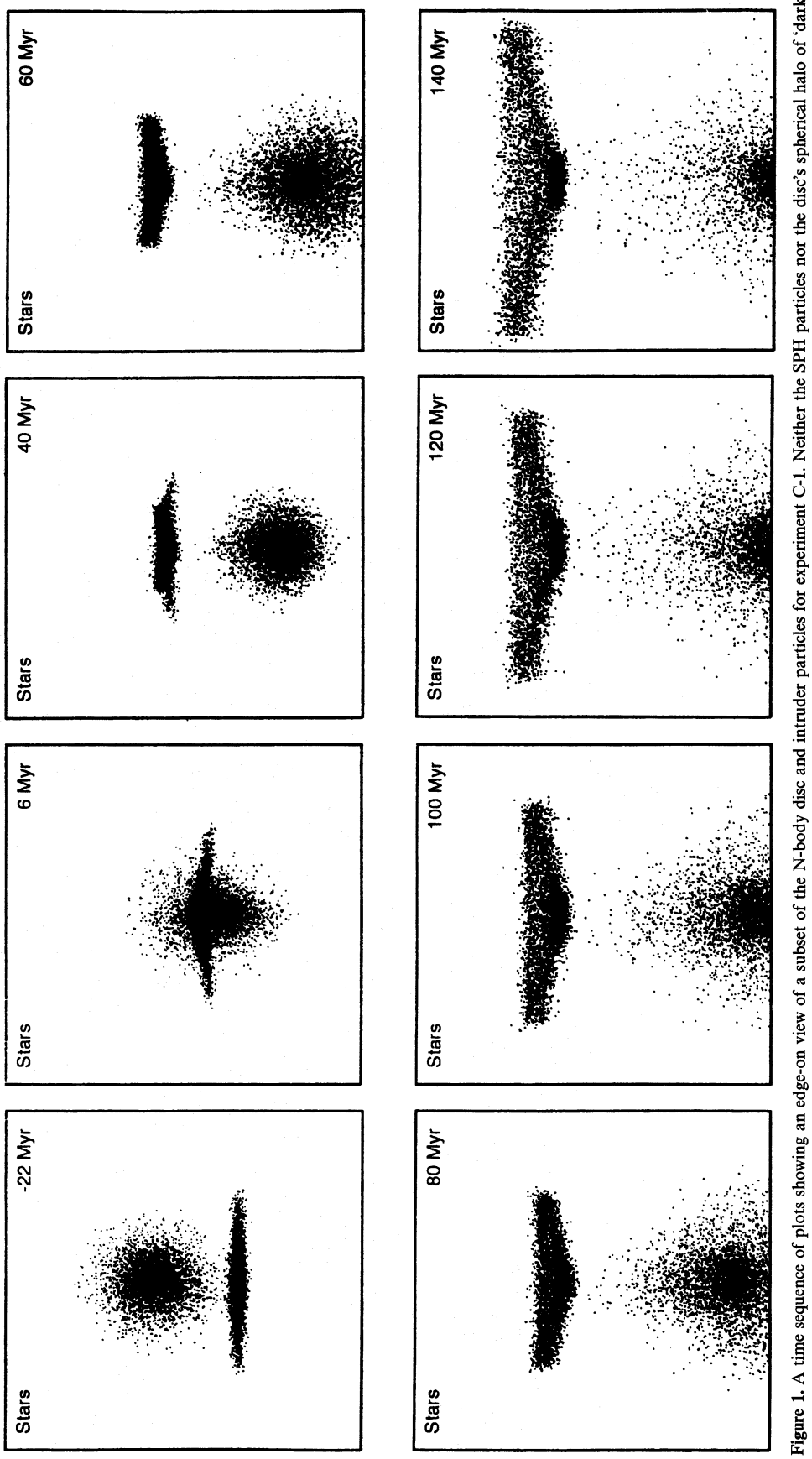


**Figure 1.** A time sequence of plots showing an edge-on view of a subset of the N-body disc and intruder particles for experiment C-1. Neither the SPH particles nor the disc's spherical halo of 'dark matter' is depicted. Time is given using the scaled unit given in the text. The two galaxies' centres of mass overlap at the zero of time.

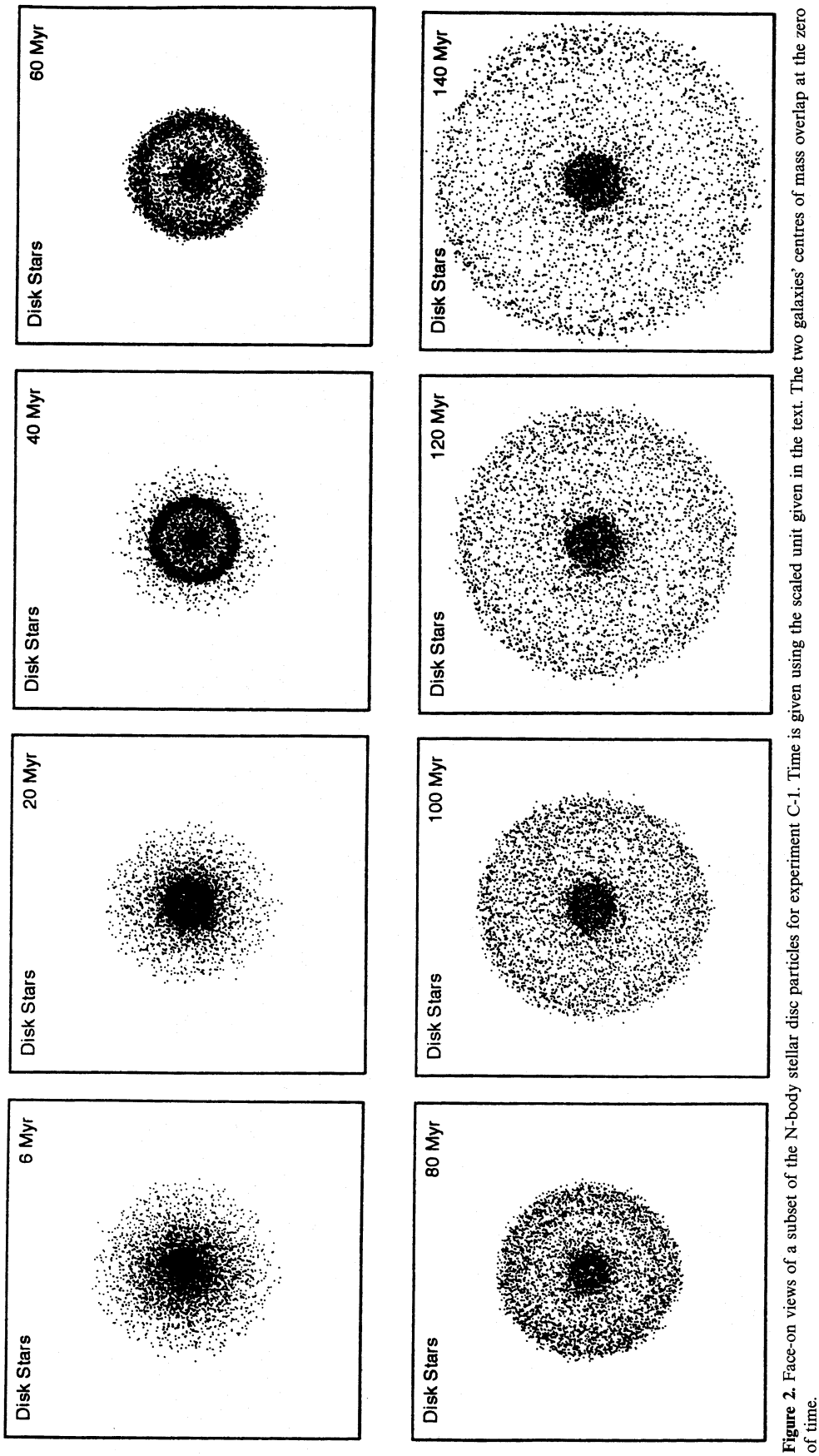


**Figure 2.** Face-on views of a subset of the N-body stellar disc particles for experiment C-1. Time is given using the scaled unit given in the text. The two galaxies' centres of mass overlap at the zero of time.

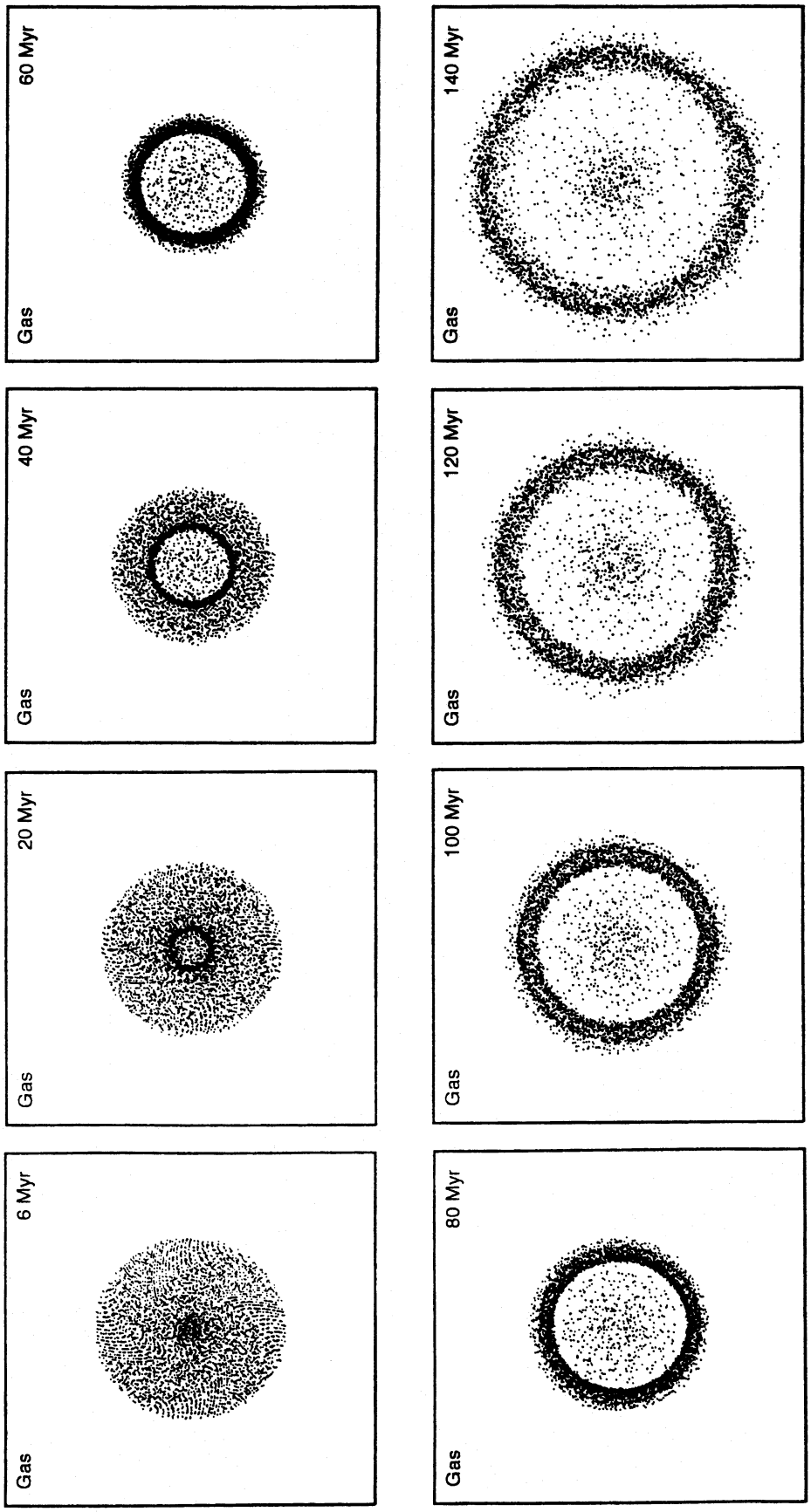


**Figure 3.** Face-on views of a subset of the SPH particles for experiment C-1. Notice that the particle density in the upper SPH plot does not necessarily indicate the gas density because the SPH particles do not all have the same mass and the three-dimensional structure is not depicted. Time is given using the scaled unit given in the text. The two galaxies' centres of mass overlap at the zero of time.

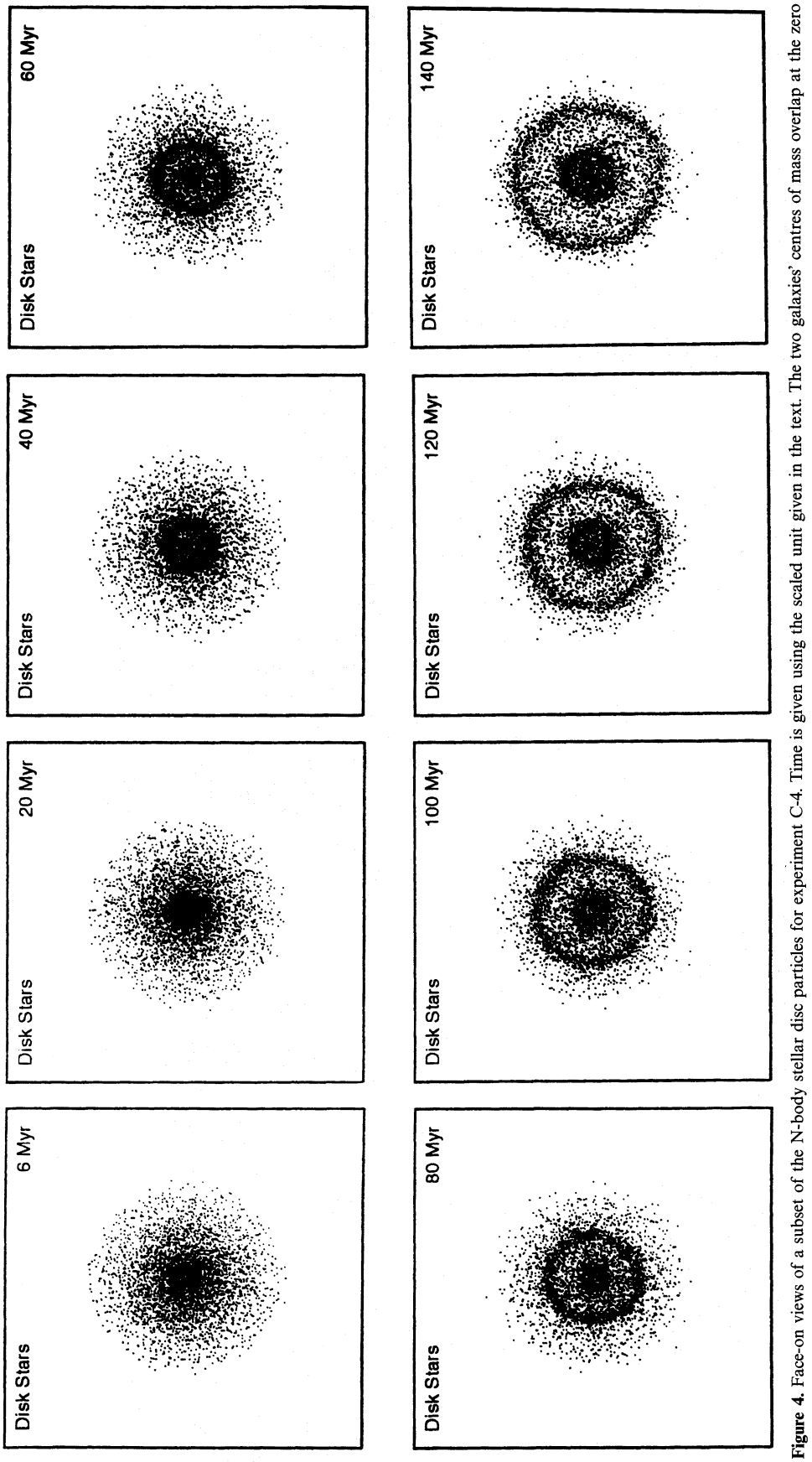


**Figure 4.** Face-on views of a subset of the N-body stellar disc particles for experiment C-4. Time is given using the scaled unit given in the text. The two galaxies' centres of mass overlap at the zero of time.

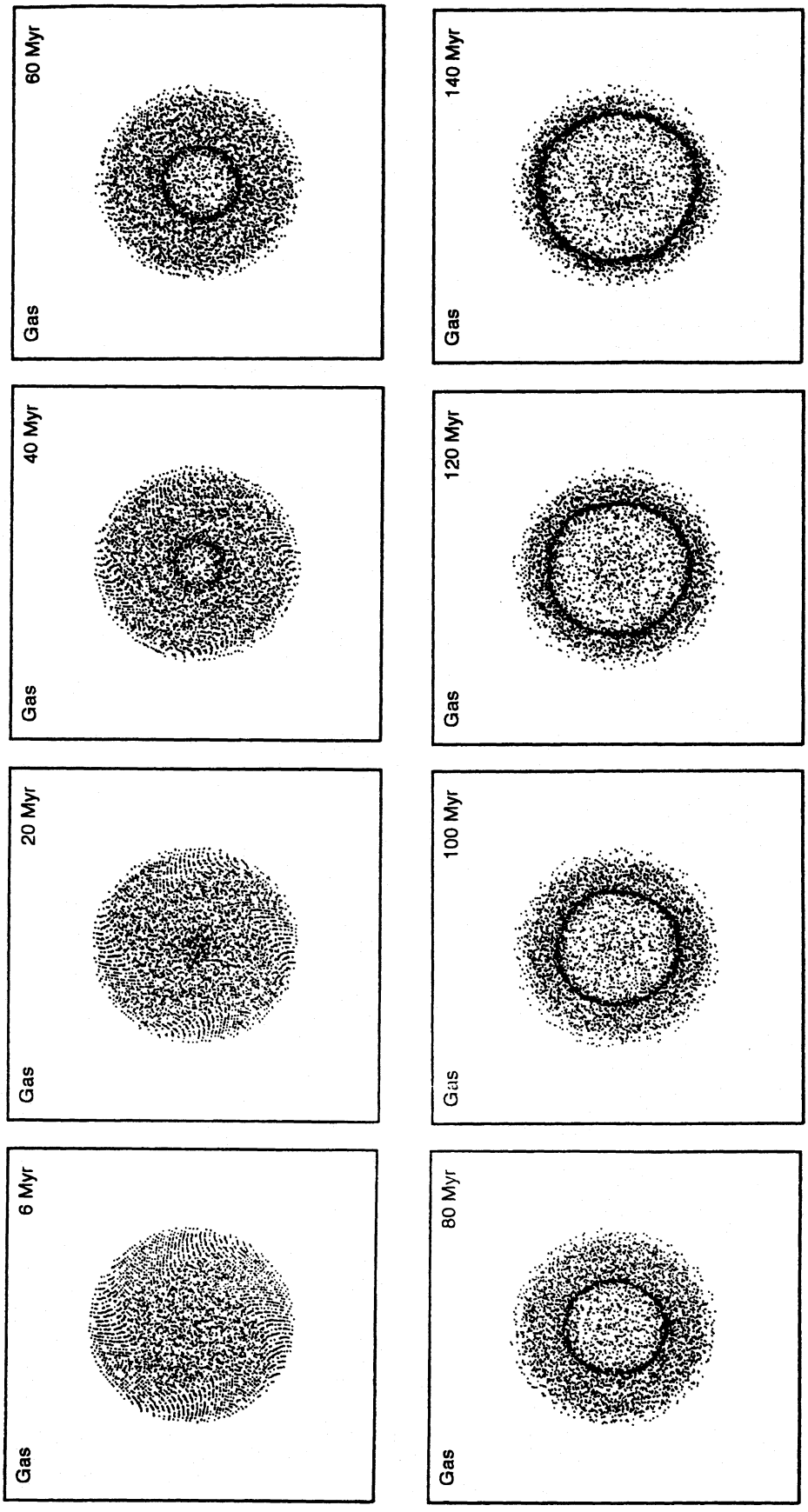


**Figure 5.** Face-on views of a subset of the SPH particles for experiment C-4. Notice that the particle density in the upper SPH plot does not necessarily indicate the gas density because the SPH particles do not all have the same mass and the three-dimensional structure is not depicted. Time is given using the scaled unit given in the text. The two galaxies' centres of mass overlap at the zero of time.

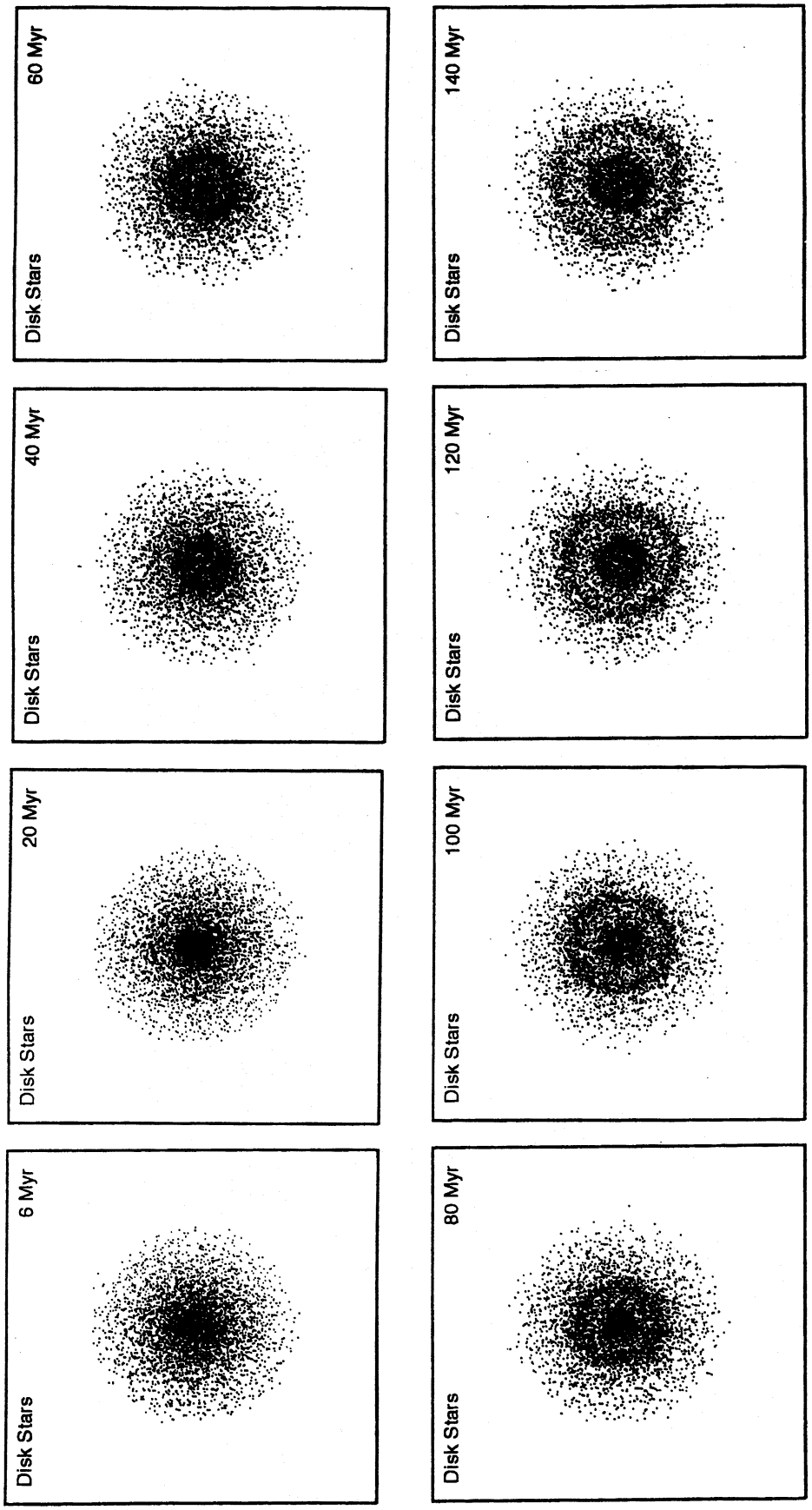


**Figure 6.** Face-on views of a subset of the N-body stellar disc particles for experiment C-10. Time is given using the scaled unit given in the text. The two galaxies' centres of mass overlap at the zero of time.

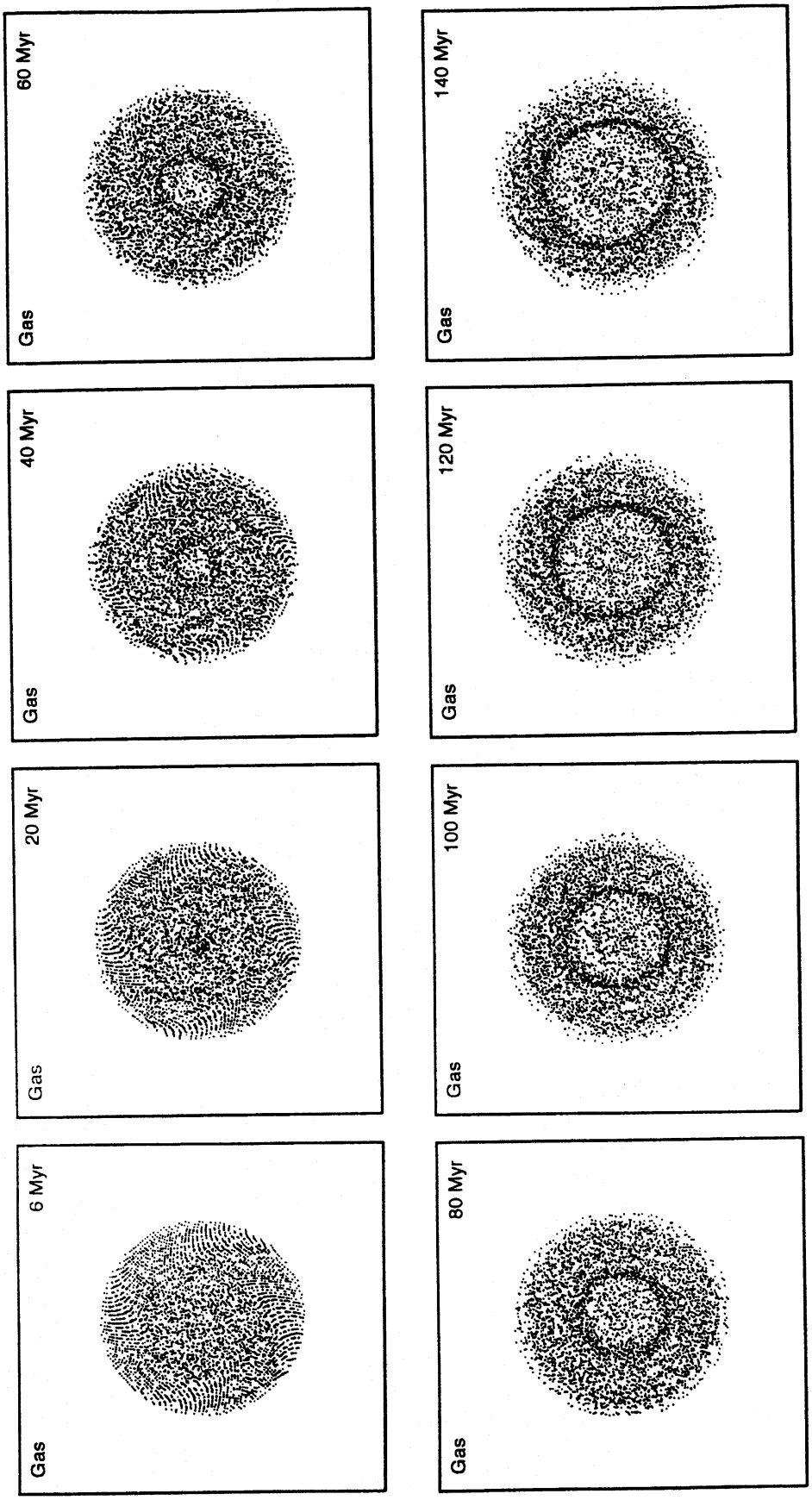


**Figure 7.** Face-on views of a subset of the SPH particles for experiment C-10. Notice that the particle density in the upper SPH plot does not necessarily indicate the gas density because the SPH particles do not all have the same mass and the three-dimensional structure is not depicted. Time is given using the scaled unit given in the text. The two galaxies' centres of mass overlap at the zero of time.

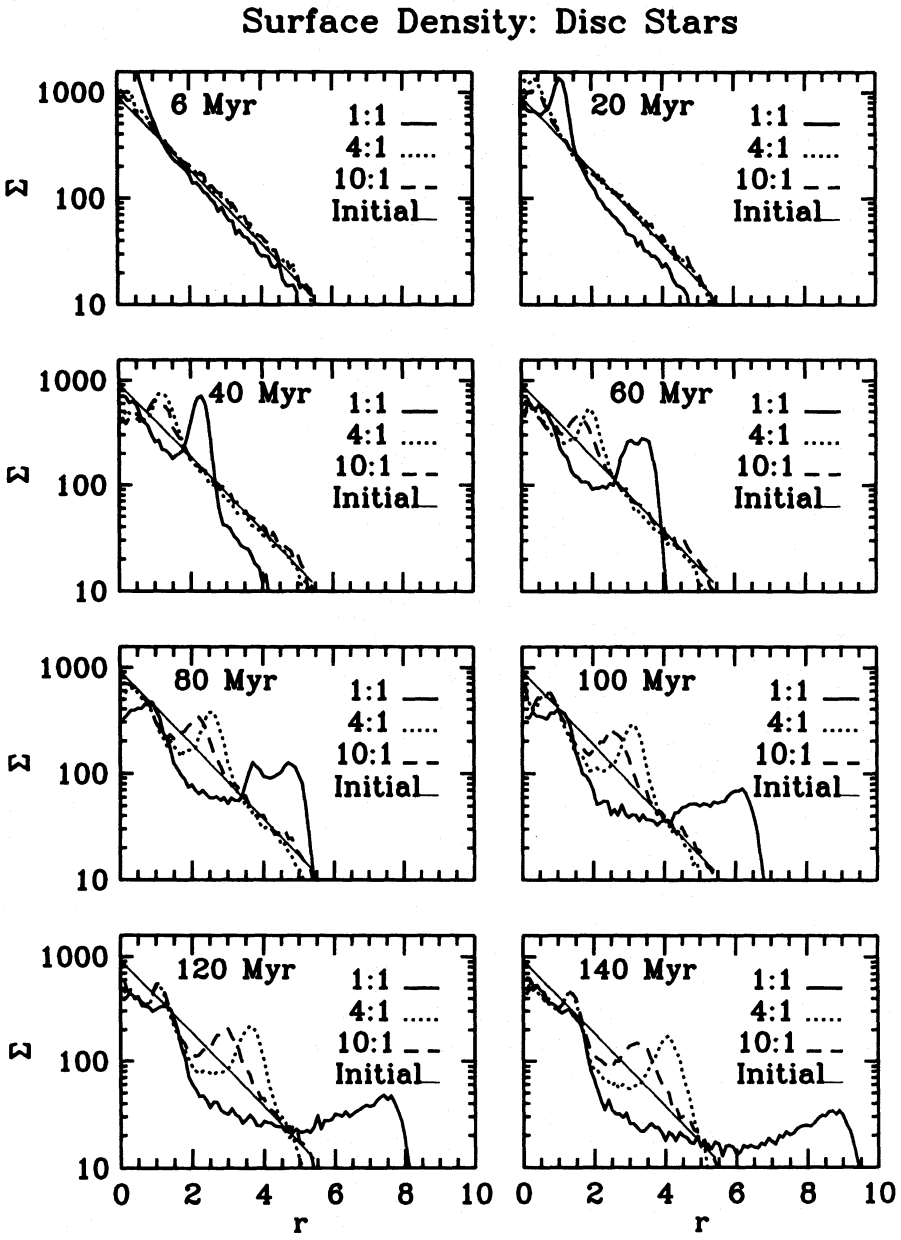


**Figure 8.** The azimuthally averaged surface density of disc stars. The density profile of the initial disc is indicated by the solid line. Using the scaling given in the text, 1000 on the plot corresponds to approximately 500 $M_{\odot}$ $pc^{-2}$.

tures since the gas (1) is collision-dominated and (2) has no radial velocity dispersion in the initial galaxy model. When the ring first forms the gaseous and stellar rings coincide in radius, but the density maxima of the two components separate later in the ring evolution. In experiment C-1, expansion of the gaseous ring lags that of the stellar ring since strongly dissipational shocks rob kinetic energy from the gas, causing it to fall behind in radius.

The behaviour of the gas in experiments C-4 and C-10 is qualitatively different. As the ring expands the narrow gaseous ring is contained within the broader stellar ring, but the density maximum of the gas ring lies on the outer edge of the stellar ring. The physical reason this occurs is because the stars are collisionless and the gas is collisional. The stellar ring is broadened by a large radial velocity dispersion as inwardly and outwardly moving stars stream past one another; however, inwardly moving gas is unable to penetrate the ring and piles up on the outer edge. Since the relative velocity between inward and outward moving gas streams is less than in experiment C-1, dissipation is less effective and the gas ring does not lag the stellar ring at this point in the overall expansion.

The planar character of the disc is destroyed by the equal-mass intruder in experiment C-1. When the inner part of the disc expands radially, it does so displaced laterally from the outer portion. The two opposing streams of material do not meet head-on in a plane; instead stars and gas move somewhat

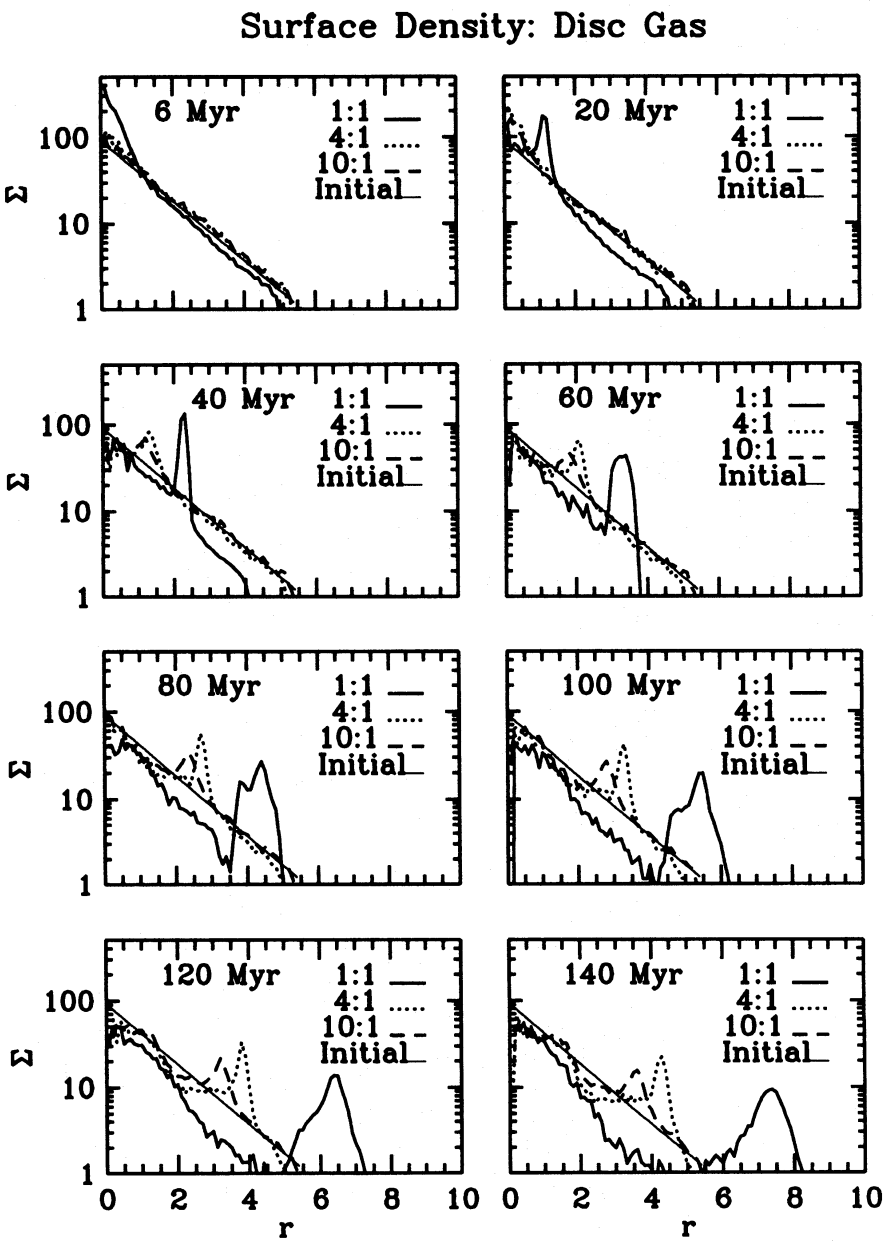


**Figure 9.** The azimuthally averaged surface density of the disc gas. The density profile of the initial disc is indicated by the solid line. Using the scaling given in the text, 100 on the plot corresponds to approximately $10^{-2}$ g cm$^{-2}$ or $6 \times 10^{21}$ H cm$^{-2}$.

in a toroidal flow in the vicinity of the ring (as Lynds & Toomre (1976) had speculated would occur). The incoming gas and outgoing gas meet and form a shock on the underside of the disc. The shocked gas is swept up and carried out with the outflowing material. The intruders in experiments C-4 and C-10 have much less effect on the vertical structure of the disc and a vertical separation of inflowing and outgoing material is not observed in these simulations.

The interaction in experiment C-1 significantly dislodges the nucleus from the plane of the ring. This permits the nucleus easily to appear displaced from the centre of the ring, as is so often observed in ring galaxies (cf. Theys & Spiegel 1976; Few & Madore 1986), even in this central collision. Much of the disc material is spread out in the direction perpendicular to the original disc plane, especially in the nucleus. However, the intruder does not capture any of the disc stars or gas in these mildly hyperbolic collisions.

### 3.2 Disc density

The development of the ring is graphically represented in the surface density plots of Figs 8 and 9. The surface density is calculated as a function of radius by integrating the mass density in the direction perpendicular to the disc and averaging over azimuthal angles. The plots show the large flow

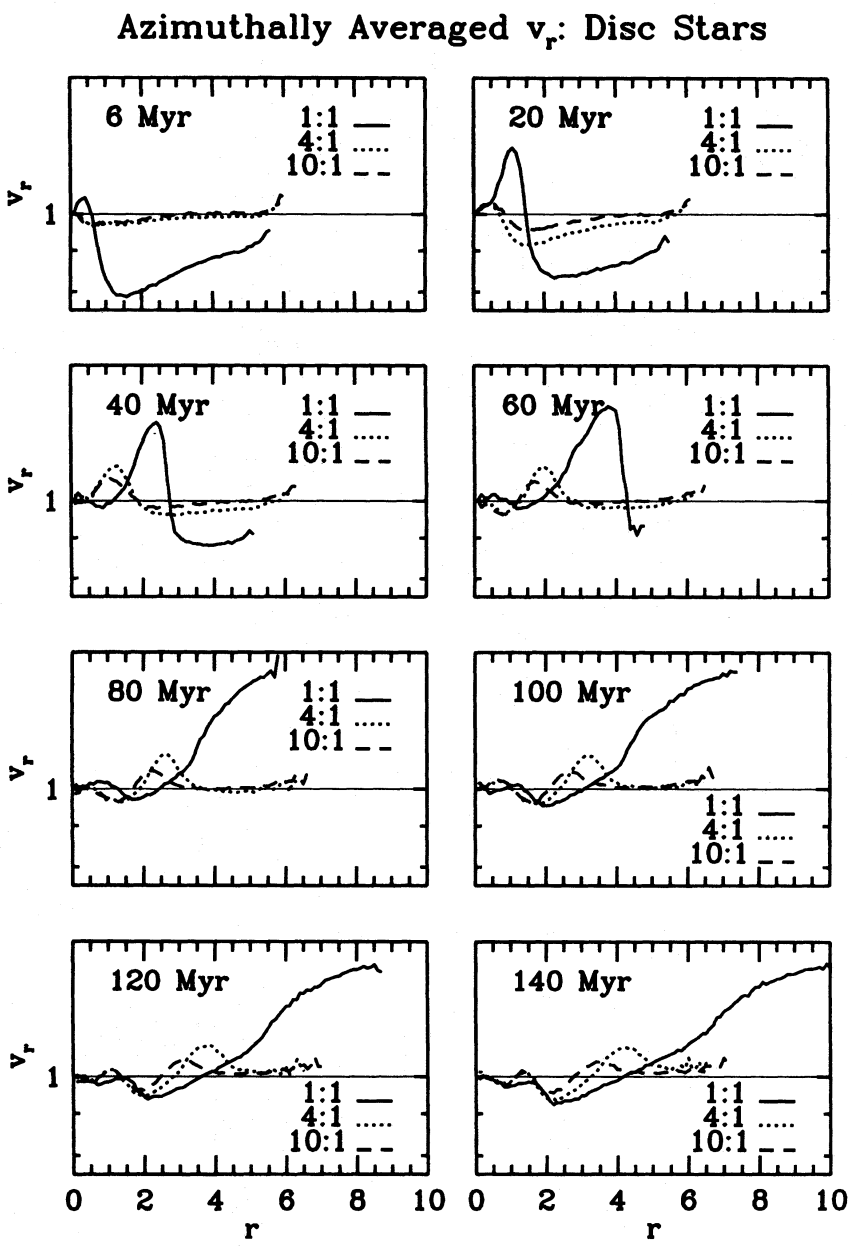


**Figure 10.** Average radial velocity as a function of radius for the disc star particles. Unity in simulation units scales to 1615 km $s^{-1}$ using the values given in the text, so the plotted velocities range from −162 km $s^{-1}$ to +242 km $s^{-1}$.

of material, first to the centre, and then to large radii for experiment C-1. At the end of the run (140 Myr), the surface density over the initial extent of the disc is well below its original value. The wave character of the ring in experiments C-4 and C-10 can be seen as the surface density oscillates about the intial value. The outer ring in experiment C-4 expands faster than the C-10 outer ring, although the inner rings in C-4 and C-10 coincide in radius at similar times after the collision.

The maximum ring surface density is greatest in experiment C-1 and is smallest in experiment C-10. In C-1 it is greater than it was in the unperturbed disc by factors of about 3–4 for the stars and 4–8 for the gas. In experiment C-10 the surface density in the ring is approximately a factor of two greater than its initial value. The contrast between the stellar and gaseous surface densities is diminished in the unequal-mass collisions. For experiment C-10, both the gas and stellar ring surface densities increase by about the same factor relative to their initial values.

Due to motion in the direction perpendicular to the disc, the three-dimensional space density is not necessarily proportional to an integrated surface density everywhere in the disc, especially in experiment C-1. For example, a compression in the direction perpendicular to the disc would not lead to a surface density increase. An examination of the three-dimensional gas density at the position of the SPH particles

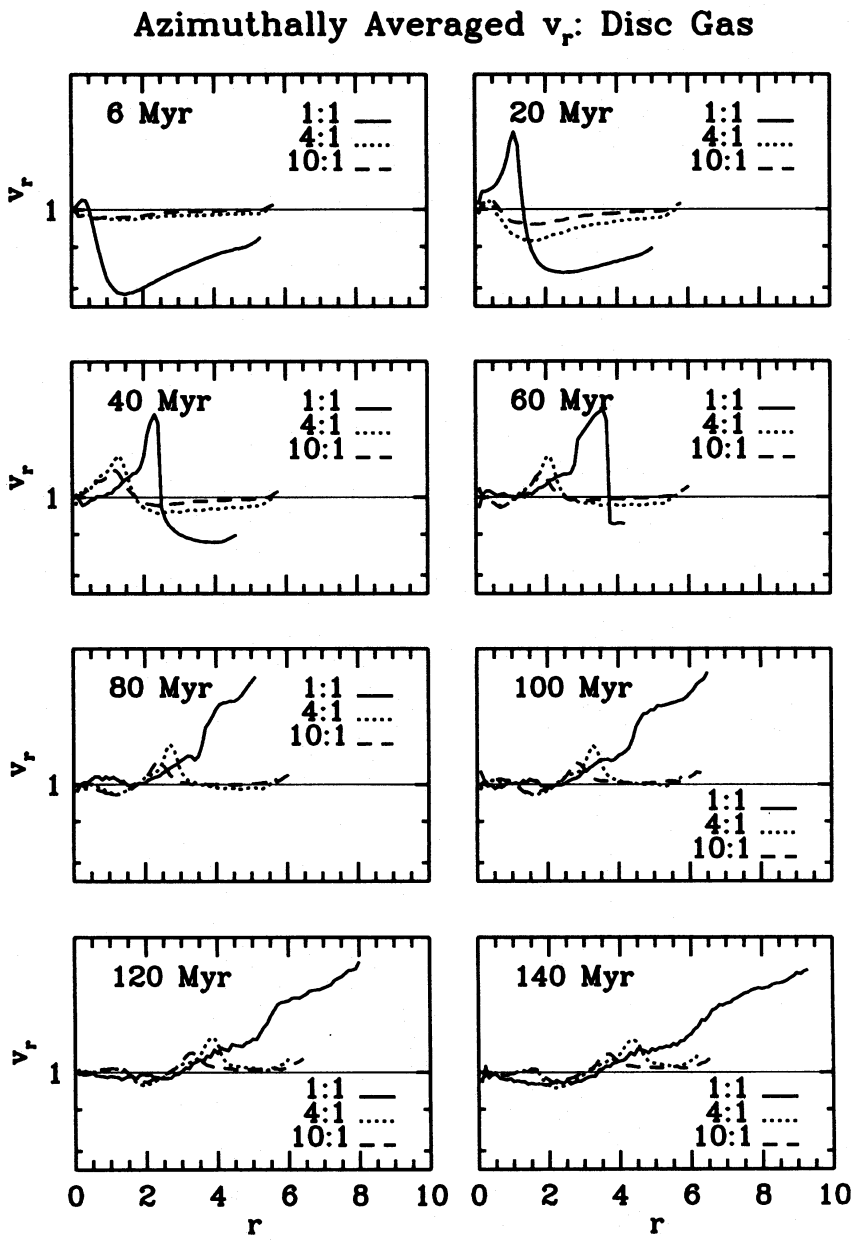


**Figure 11.** Average radial velocity as a function of radius for the SPH particles. Unity in simulation units scales to 1615 km $s^{-1}$ using the values given in the text, so the plotted velocities range from −162 km $s^{-1}$ to +242 km $s^{-1}$.

reveals that the true (3D) gas density in the ring remains greater than that in the nucleus until 100 Myr. The surface density, however, has fallen below that in the nucleus after 60 Myr. The discrepancy occurs because gas is spread vertically in the centre to a greater extent than it is in the ring.

In the central regions the maximum density is attained quickly after passage of the intruder, the three-dimensional density values rising by approximately a factor of five in experiment C-1. As the ring forms and moves outward through the disc, the relative three-dimensional gas density increases by even larger factors. In experiment C-1 a maximum increase of a factor of 10–20 occurs at 40 Myr.

### 3.3 Halo and intruder response

Some of the difference between the equal-mass collision and the other two experiments can be attributed to the behaviour of the halo. In experiment C-1 the halo becomes quite disrupted and the disc and halo expand greatly. Comparitively little damage is done to the halo in experiments C-4 and C-10. This expansion of the halo in experiment C-1 has the further effect of lowering the rotation curve for the disc particles at the end of the run (see Figs 12 and 13 later).

We do not follow the intruder for long in these experiments, allowing it to fall off the edge of the computational box. Based on the fate of the halo, however, we would expect

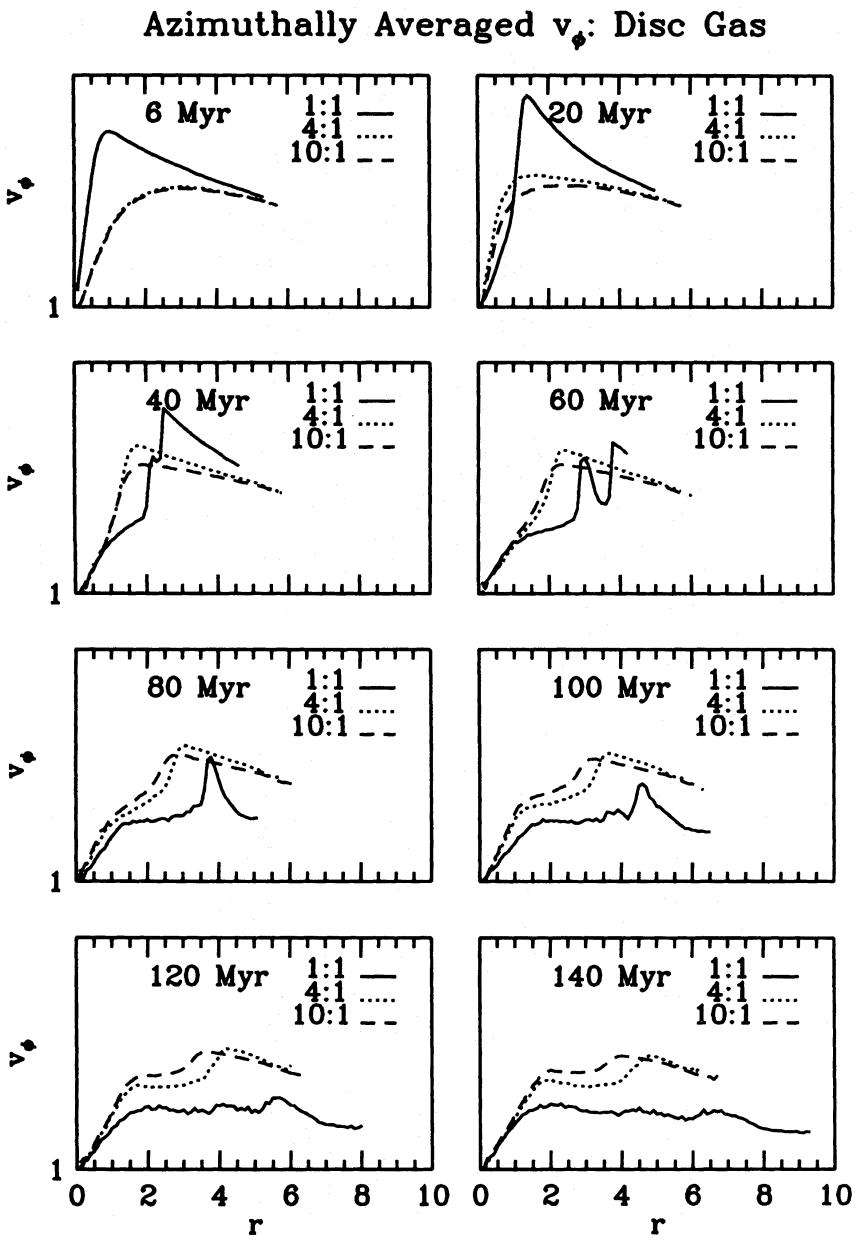


**Figure 12.** Average azimuthal velocities as a function of radius for the SPH particles. Unity in simulation units scales to 1615 km s$^{-1}$ using the values given in the text, so the plotted velocities range from 0 km s$^{-1}$ to 485 km s$^{-1}$.

that it could become quite disrupted and may suffer significant mass loss from such a collision. This suggests that the intruders often associated with observed ring galaxies may have lost significant numbers of stars and may have been more massive prior to the collision.

### 3.4 Velocities

Radial velocities in radial bins as calculated by

$$< v_R >= \frac{\sum_i m_i (v_R)_i}{\sum_i m_i},$$

where the sum is over all particles, are shown in Figs 10 and 11. Very large inflow and expansion velocities are attained in experiment C-1. For this experiment the radial velocities are all positive (outward) near the ring. Even at the end of the run at 140 Myr, the particles at the edge of the disc show little sign of slowing down, although by the end of the experiment the radial velocity of the gas lags that of the disc stars by approximately 50 km s$^{-1}$. In experiments C-4 and C-10, the radial velocity becomes negative right behind the ring.

Azimuthal velocities are plotted in Figs 12 and 13. The passage of the intruder gives the particles an inward pull and angular momentum conservation demands that azimuthal velocities increase accordingly. (Angular momentum transfer due to artificial shear viscosity is relatively small.) The initial

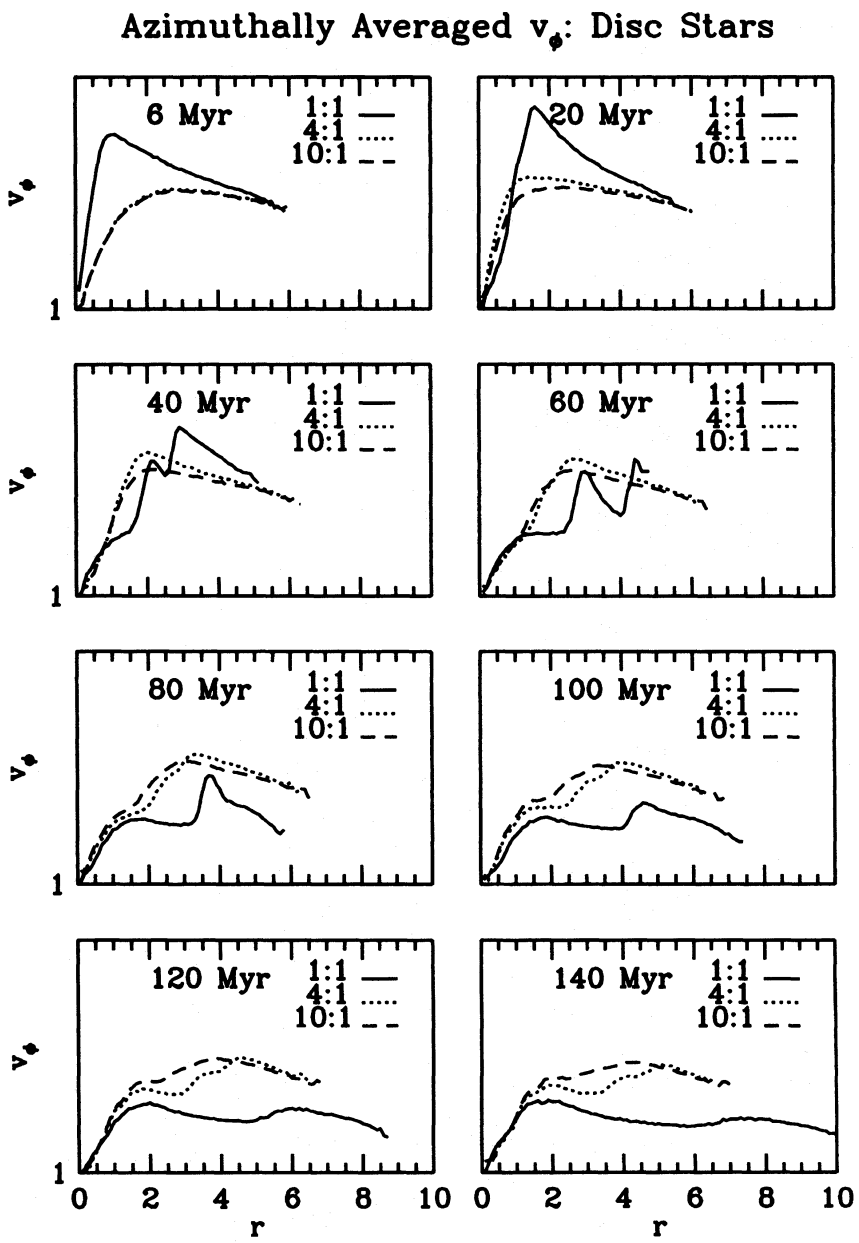


**Figure 13.** Average azimuthal velocities as a function of radius for the star disc particles. Unity in simulation units scales to 1615 km s$^{-1}$ using the values given in the text, so the plotted velocities range from 0 km s$^{-1}$ to 485 km s$^{-1}$.

peak in the velocity curve of a scaled 250 km s$^{-1}$ increases to about 450 km s$^{-1}$ at 20 Myr for experiment C-1. That value declines during the expansion; the velocity curve behind the ring is flat over much of the disc at 140 Myr and lower than that for the unequal-mass collisions owing to the large radial displacement of material and the expansion of the halo.

At 60 Myr in experiment C-1, the azimuthal velocity curve for the stars has a depression near the ring. These low values are due to a dense group of particles which came from small radii and have had to slow their azimuthal velocity in order to conserve angular momentum. The depression in the gas plot stems from the same cause, but this is only possible due to the three-dimensional nature of the flow near the ring. The outgoing outer part of the ring is able to expand displaced laterally from the infalling material. The inner and outer parts of the disc actually meet interior to the ring's outer edge. Similar behaviour is not seen in experiments C-4 and C-10 where the disc remains approximately planar.

## 4 DISCUSSION

The three experiments presented here show how changing the mass ratio between the two galaxies affects the ring formation and development. The equal-mass collision in experiment C-1

greatly disrupts the disc galaxy and its halo. The disc is significantly warped out of its planar configuration, leading to a complex flow of material near the ring. Ring expansion occurs at a slower pace and the velocities involved are lower as the mass ratio increases.

An interesting result of the equal-mass collision (C-1) is that any inner stellar ring structure is difficult to discern for as long as the interaction is followed, by which time the outer ring has become quite diffuse. A hint of an inner ring can be seen in Fig. 8 which shows the surface density as a function of radius, but the surface density is less than that in the initial disc. It is possible that a higher resolution simulation may enhance the inner ring structure, however.

With a less massive intruder, an inner ring develops while the outer ring is still prominent. The inner ring is primarily a stellar feature, which also appears to be the case for the inner observed ring in the Cartwheel galaxy (Marcum et al. 1992). Inner rings are predicted by analytic studies of small-amplitude disturbances (Appleton & Struck-Marcell 1987a; Struck-Marcell & Appleton 1987), and are present in the simulations of Huang & Stewart (1988) and Toomre (1978). The models of Stuck-Marcell & Higdon (1993), Hernquist & Weil (1993), and Mihos & Hernquist (1994) also develop prominent inner rings while the outer rings are still present. More experiments are needed to determine the precise conditions under which inner and outer rings coexist.

In the simulations by Hernquist & Weil (1993), Stuck-Marcell & Higdon (1993), and Mihos & Hernquist (1994), spoke-like features are seen to develop, similar to those seen in the Cartwheel galaxy. No obvious spokes are evident in any of the models discussed here. It is likely that other models developed spokes because, compared with the present model, (1) cooler gas was used and (2) initial disc models were used that, prior to the collision, had developed significant clumpy internal structure, which served as a seed to spoke formation.

The collisionless N-body experiments of Huang & Stewart (1988, HS) are in general agreement with the present series of experiments. HS used a rigid intruder of mass 0.4 that of the disc galaxy. The magnitude of the surface density enhancement in the central collision of HS is less than that in model C-1, by what appears to be a factor of approximately two, but is slightly greater than we measured in model C-4. The radial velocities in HS exhibit the same characteristic increase with radius at later times of the expansion. The disturbance of the disc in the vertical direction is relatively minor in HS's experiments; it appears that an intruder of nearly equal mass is needed to produce significant lateral separation of infalling and expanding material. HS also noted that the halo has an important dynamical effect on the evolution of the ring. As is also seen in present experiments, use of a 'live' halo enhances the expansion of the ring.

In making comparisons between the models and observations of real galaxy systems it is necessary to distinguish between the old stellar population present prior to the collision and young stars formed as a result of the collision. The old stellar population is best detected in the near-infrared and such observations of colliding galaxies (see Bushouse & Stanford 1992) generally show less morphological disturbance than is displayed in the optical morphology where young stars and hot gas dominate the emission. Presumably the latter delineates those regions of the galaxy in which gas has been concentrated leading to significant recent star formation.

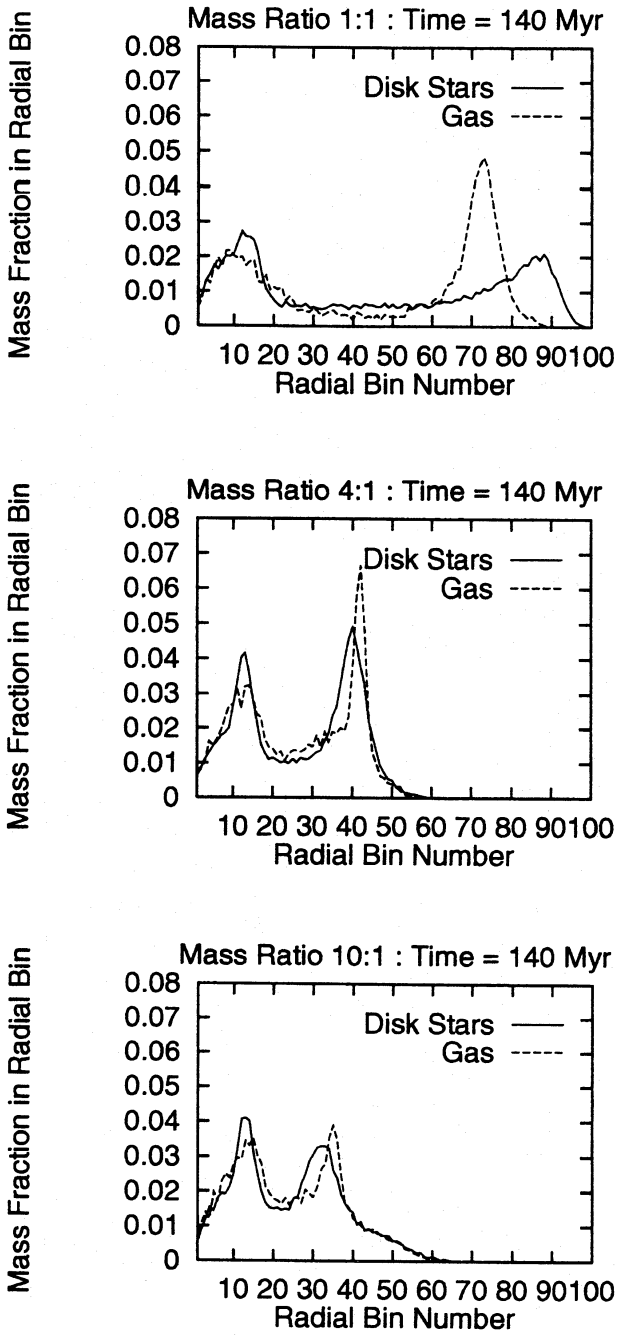


**Figure 14.** The fraction of the total mass of each component contained in each bin, which are equally spaced in radius.

Qualitatively, observations are in agreement with the present model. For instance, the *R*-band (red) surface brightness of the broad ring in VII Zw 466 is approximately a factor of 15 greater than that inside the ring (Thompson & Theys 1978). Just outside the ring the brightness falls by at least a factor of 100. This observed magnitude difference is much greater than we would predict if the *R* band probed only the background disc mass, but recent star formation also shows up at *R*. The observations, together with our models, are consistent with the hypothesis that a significant amount of

star formation was triggered by the interaction, and that the resulting stellar population has aged about $10^7$ yr.

The precipitous decline in surface brightness just outside the ring is also seen in a number of well-observed ring systems (Marston & Appleton 1995). This could indicate that these rings are well developed and have expanded beyond the 'edge' of the initial disc. In systems with no observed inner ring, our models would suggest that the intruder was quite massive, although it is also possible that we are viewing systems in which the first, outer ring has already dispersed.

Marston & Appleton (1995) have recently reported observations of a sample of ring galaxies which show that the Hα distribution is strongly peaked at the outer edge of the rings, and embedded in a more extended ring of old stars. These observations are consistent with our models C-4 and C-10, but not with experiment C-1. Fig. 14 shows the relative mass fraction of each component (gas and stars) contained in concentric radial bins at 140 Myr following the collision.

It is difficult simply to scale the measured surface density in our experiments to observed fluxes and star formation rates since induced star formation can significantly alter the observed surface brightness. The details of the small-scale sequence of events that lead to the observed bursts of star formation in the rings are unknown. However, it is observed that enhanced star formation is associated with the arms of spiral galaxies (e.g., Roberts 1969) and these arms are locations of elevated gas density and shock fronts. By analogy, it can be argued that regions of high gas density and shocks are likely sites for star formation, at least for the bright OB associations and H II regions which highlight spiral structure (Mouschovias et al. 1974) and observed rings.

Relatively little is known quantitatively about how star formation rates scale with either gas density increases or shock strengths under the conditions we are considering. One prescription for non-interacting galaxies is that given by Schmidt (1959) in which the star formation rate scales with the local gas density to a power, $n$. Schmidt (1959) and Field & Saslaw (1965) argue for $n$=2, and Kennicutt (1989) finds $n$=1.3 with a lower density cut-off. Mihos & Hernquist (1994) model star formation using a Schmidt Law with $n$=1.5.

The Schmidt Law can be used to estimate star formation rate increases from the model data. If it is assumed that the pre-collision disc was producing stars at some background rate, then the relative increase in gas density can be used to derive an enhanced rate relative to the background one. Since the peak relative density increase in the ring for experiment C-1 is on the order of 20, use of the Schmidt Law with $n$=1.3 allows a prediction of a star formation rate increase of a factor of approximately 50.

However, in order to compare a predicted star formation rate increase with observations it would be necessary to integrate the star formation rate over time-scales relevant to the wavelength regimes in which observations are obtained. For example, observations with *IRAS* sample both the massive star contribution (as reprocessed through dusty regions in the vicinity of the stars) and the older underlying stellar population which contributes to the overall radiation field and illuminates large-scale 'cirrus' clouds. The estimated increases in star formation rate of 50 may not translate into such large changes in the far-infrared flux as observed by *IRAS* . There may also be a dilution effect in that *IRAS* resolution permits only global measurements and $L_{\rm FIR}$ could increase greatly in regions of active star formation. The factor of 2 in the ratio of $L_{\rm FIR}/L_B$ obtained by Appleton & Struck-Marcell (1987a) in their *IRAS* study of ring galaxies is consistent with that found in other optically selected colliding galaxies (Bushouse, Lamb & Werner 1988).

We can try to test the hypothesis that star formation occurs in regions of strong gas interactions and high gas densities in a qualitative manner using the present experiments. The Cartwheel galaxy is the best observed ring galaxy (Higdon 1993; Struck-Marcell & Higdon 1993; Marcum et al. 1992; Fosbury & Hawarden 1977) and, while none of the three experiments presented here is an exact match, experiment C-4 is somewhat analogous. In the Cartwheel galaxy, the outer portion of the outer ring is observed to be bluer than the inner part (Marcum et al. 1992), as we would expect since, in our model of low-mass companions, the gas piles up at the outer edge of the ring, and the Cartwheel's companion is thought to have a low mass (Fosbury & Hawarden 1977, but see the discussion below about the intruder's original mass).

Model C-4 and the Cartwheel have a number of additional similarities. At 140 Myr in experiment C-4, the ratio of the diameter of the outer and inner rings is 4:1, compared with 4.7:1 in the Cartwheel (Higdon 1993). The gas radial velocity curve in model C-4 has the same approximate shape as determined by Higdon (1993), and the model expansion velocity peaks at 65 km s$^{-1}$ compared to the Cartwheel value of 61 km s$^{-1}$. The infall velocity behind the ring is 32 km s$^{-1}$ in the model versus 35 km s$^{-1}$ in the Cartwheel. The largest discrepancy is between the observed H I circular velocity curve and the gas azimuthal velocity curve in experiment C-4. The Cartwheel's H I velocity rises linearly from $\approx$ 70 km s$^{-1}$ at a radius of 3 kpc to a value of $\approx$ 300 km s$^{-1}$ at a radius of 17 kpc. The azimuthal velocity for experiment C-4 rises from 65 km s$^{-1}$ at 3 kpc to a peak of $\approx$ 235 km s$^{-1}$ at 13 kpc and the rise is not linear (see Fig. 13).

Given all these similarities and the linear size and the ring spacing of the Cartwheel, our experiment suggests that the intruder to disc galaxy mass ratio was on the order of 4:1 or less, which was also an approximate criterion necessary to produce spokes in the simulations of Hernquist & Weil (1993). Observations indicate that all three galaxies near the Cartwheel are much less massive than this. One possible explanation is that the intruder was originally more massive, but suffered considerable mass loss during the encounter.

The lack of a strong inner gaseous ring in our experiments stands counter to the results of Hernquist & Weil (1993) and Mihos & Hernquist (1994). The Cartwheel has little or no gas and star formation in its inner stellar ring, which is consistent with the results presented here. The source of the discrepancy is under investigation (see Gerber 1994).

We point out one issue concerning the age of the ring. In making age estimates of observed rings the measured expansion velocity in the ring is taken as a constant in time and extrapolation is done backwards to determine the approximate ring age. If we do this for experiment C-4 at $T$=140 Myr, we obtain

$$\tau = \frac{13\,\mathrm{kpc}}{65\,\mathrm{km\ s^{-1}}} \approx 195\,\mathrm{Myr},$$

an error of nearly 40 per cent. This implies that the Cartwheel ring may be younger than the 260 Myr estimated by Higdon (1993).

## 5 SUMMARY

The collision of a spherical galaxy with a disc galaxy, where the spherical intruder hits the centre of the disc at normal incidence, leads to the formation of an expanding ring of stars and gas.

When the two galaxies are of equal mass, both systems are significantly disrupted, and the resulting ring contains a large amount of disc material. The surface density of both gas and stars on both sides of the ring is depressed below its original value. Scaling to the mass of a typical spiral galaxy, the expansion velocity of the ring is on the order of 180 km $s^{-1}$ and the rotation speed of particles in the ring can reach values of 450 km $s^{-1}$. Owing to dissipational interactions, the gaseous ring expands slower than the stellar ring. The disc is significantly deformed from its original planar configuration.

If the intruder galaxy is one-fourth or less as massive as the disc galaxy, the stellar ring propagates outward as a density wave. A thin gaseous ring forms at the leading edge of the stellar ring. Lower mass companions produce less dense rings and less perturbed velocity fields. An inner ring of stars forms while the outer ring is still prominent. The outer ring expands more slowly with less massive intruders.

## ACKNOWLEDGMENTS

The authors thank C. Struck and P. Appleton for helpful discussions. We gratefully acknowledge the support of NASA graduate student training grant NGT 70041, NASA grant NAG5-1241, and University of Illinois Research Board grants. Computer time allocations were granted through the National Center for Supercomputing Applications (NCSA) at the University of Illinois and the Numerical Aerodynamic Simulation (NAS) facility at NASA Ames Research Center. Numerical calculations were performed at NCSA and NAS. RG also gratefully acknowledges support from a National Research Council postdoctoral fellowship.

## REFERENCES

Appleton P. N., Struck-Marcell C., 1987a, ApJ, 312, 566
Appleton P. N., Struck-Marcell C., 1987b, ApJ, 318, 103
Bahcall J. N., Soneira R. M., 1980, ApJS, 44, 73
Balsara D. S., 1990, Ph.D. thesis, University of Illinois at Urbana-Champaign
Barnes J. E., 1988, ApJ, 331, 699
Binney J., Tremaine S., 1987, Galactic Dynamics. Princeton University Press, Princeton, NJ
Bushouse H. A., Lamb S. A., Werner M. W., 1988, ApJ, 325, 74
Bushouse H. A., Stanford S. A., 1992, ApJS, 79, 213
Few J. M. A., Madore B. F., 1986, MNRAS, 222, 673
Field G. B., Saslaw W. C., 1965, ApJ, 142, 568
Fosbury R. A. E., Hawarden T. G., 1977, MNRAS, 178, 473
Gerber R. A., 1993, Ph.D. thesis, University of Illinois at Urbana-Champaign
Gerber R. A., 1994, BAAS, 26, 1430
Gerber R. A., Lamb S. A., 1994, ApJ, 431, 604
Gerber R. A., Lamb S. A., Balsara D. S., 1992, ApJ, 399, L51
Gilmore G., Wyse R. F. G., Kuijken K., 1989, ARA&A, 27, 555
Gingold R. A., Monaghan J. J., 1977, MNRAS, 181, 375
Gingold R. A., Monaghan J. J., 1981, MNRAS, 197, 461
Gingold R. A., Monaghan J. J., 1982, J. Comput. Phys., 46, 429
Hernquist L., Katz N., 1989, ApJS, 70, 419
Hernquist L., Weil M. L., 1993, MNRAS, 261, 804
Higdon J. L., 1993, Ph.D. thesis, University of Texas at Austin
Hockney R. W., Eastwood J. W., 1988, Computer Simulations Using Particles. Adam Hilger, Bristol
Huang S., Stewart P., 1988, A&A, 197, 14
Jeske N. A., 1986, Ph.D. thesis, University of California, Berkeley
Jog C. J., Das M., 1992, ApJ, 400, 476
Jog C. J., Solomon P. M., 1992, ApJ, 387, 152
Kennicutt R. C., 1989, ApJ, 344, 685
King I. E., 1966, AJ, 71, 64
Lattanzio J. C., Monaghan J. J., Pongracic H., Schwarz M. P., 1986, SIAM J. Sci. Stat. Comput., 7, 591
Lucy L. B., 1977, AJ, 82, 1013
Lynds R., Toomre A., 1976, ApJ, 209, 382
Marcum P., Appleton P., Higdon J., 1992, ApJ, 399, 57
Marston T., Appleton P. N., 1995, AJ, 109, 1002
Mihos C., Hernquist L., 1994, ApJ, 437, 611
Miller R. H., Smith B. F., 1980, ApJ, 235, 421
Monaghan J. J., 1992, ARA&A, 30, 543
Mouschovias T. Ch., Shu F. H., Woodward P. R., 1974, A&A, 33, 73
Noguchi M., Ishibashi S., 1986, MNRAS, 219, 305
Olson K. M., Kwan J., 1990a, ApJ, 349, 480
Olson K. M., Kwan J., 1990b, ApJ, 361, 426
Press W. H., Flannery B. P., Teukolsky S. A., Vetterling W. T., 1986, Numerical Recipes. Cambridge University Press, Cambridge
Rasio F. A., Shapiro S. L., 1991, ApJ, 368, 111
Roberts W. W., 1969, ApJ, 158, 123
Scalo J. M., Struck-Marcell C., 1986, ApJ, 301, 77
Schmidt M., 1959, ApJ, 129, 243
Sellwood J. A., 1987, ARA&A, 25, 151
Spitzer L., 1978, Physical Processes in the Interstellar Medium. Wiley, New York
Struck-Marcell C., 1990, AJ, 99, 71
Struck-Marcell C., Appleton P. N., 1987, ApJ, 323, 480
Struck-Marcell C., Higdon J. L., 1993, ApJ, 411, 108
Struck-Marcell C., Lotan P., 1990, ApJ, 358, 99
Theys J. C., Spiegel E. A., 1976, ApJ, 208, 650
Theys J. C., Speigel E. A., 1977, ApJ, 212, 616
Thompson L. A., Theys J. C., 1978, ApJ, 224, 796
Toomre A., 1964, ApJ, 139, 1217
Toomre A., 1978, in Longair M. S., Einasto J., eds, Proc. IAU Symp. 79, Large Scale Structure of the Universe. Reidel, Dordrecht, The Netherlands, p.109
Woodward P. R., 1976, ApJ, 207, 484

## APPENDIX A: INITIAL GALAXY MODELS

A steady-state representation of an unperturbed galaxy is desired before a collision experiment is undertaken. The goal is to make the model as simple as possible, while at the same time including enough detail to capture the relevant physics. We include (1) a thin disc of stars, (2) a thin disc of gas, and (3) a spherical massive halo distribution of collisionless gravitating stars and 'dark' matter. This halo is dynamically important in any interaction (see Barnes 1988; Huang & Stewart 1988) and is therefore explicitly represented with particles in the model. However, it is not practical from the standpoint of computational efficiency to include an isothermal distribution many times the size of the disc, which would match observed constant rotation curves. The compromise is to represent the halo using a spherical model with a density that falls off more quickly than $1/r^2$ at large radii, giving it a finite mass and outer radius. The exact form of the distribution is discussed further below.

The disc is represented with a surface density distribution

that matches the observed radial exponential decline in surface brightness. It is made as thin as possible given the available computational resolution. The stars are given a velocity dispersion sufficient to suppress local axisymmetric instabilities.

The galaxy that collides with the disc galaxy is represented as a gas-free spherical galaxy with an isotropic velocity dispersion (specifically, a King (1966) model).

## A1 Construction of initial models

Our starting N-body disc galaxy model is similar to those used by Barnes (1988). Hernquist (Hernquist & Weil 1993) uses an N-body/gas dynamics starting model quite similar to ours. The general procedure for building these initial models has been discussed by many authors, including Sellwood (1987) and Barnes (1988). The details of our method are discussed below.

### *A1.1 Intruder*

The intruder is represented with a spherical King model as described in Binney & Tremaine (1987) with a choice of $\Psi(0) = 3\sigma^2$, which gives a compromise between the very centrally condensed distributions observed in real galaxies and the need to keep the number of central particles relatively small for numerical reasons. This model is similar to the models of Miller (e.g., Miller & Smith 1980) which are based on a different distribution function ($n$=3 polytropes). This King model can be characterized in terms of its average density, $\bar{\rho}$, and central density, $\rho_c$=83.80 $\bar{\rho}$.

The distribution is populated with particles by dividing the King model's spherically symmetric phase space into radial bins in both position and velocity and then filling those phase-space bins. The particles are isotropically and randomly distributed in angle in both position and velocity space.

### *A1.2 Halo of disc galaxy*

Following a method similar to that described in Barnes (1988), a King model is built (as described in Section A1.1) to serve as a model for the galactic halo. So as not to perturb the halo violently by suddenly imposing a massive disc upon this model, the analytic force due to a thin exponential disc is slowly imposed over several crossing times. This method may somewhat mimic the the actual way the disc formed as it collapsed in the potential of the halo.

The potential for a two-dimensional disc of surface density $\Sigma(r) = \Sigma_0 \exp(-r/R_d)$ is (see Binney & Tremaine 1987)

$$\Phi(r,z) = -2\pi G \Sigma_0 R_d^2 \int_0^\infty \frac{J_0(kr)\exp(-k|z|)}{[1+(kR_d)^2]^{3/2}}\,dk. \qquad \text{(A1)}$$

In this expression $J_0$ is the zeroeth Bessel function and $R_d$ is a constant. The integral is made dimensionless by defining $\xi \equiv kR_d$, $\omega \equiv r/R_d$, and $\zeta \equiv z/R_d$. Then

$$\Phi(\omega,\zeta) = -\frac{G M_{exp}}{R_d} \int_0^\infty \frac{J_0(\omega\xi)\exp(-\zeta\xi)}{[1+\xi^2]^{3/2}}\,d\xi \qquad \text{(A2)}$$

where $M_{exp}$ is the mass of the infinite exponential disc, $M_{exp}=2\pi\Sigma_0 R_d^2$. The integral is evaluated numerically and a table of values in $r$–$z$ space is produced. At each time step a subroutine to the main program calculates the force at the position of each particle by simple differencing of the tabulated potential values. This force is then added to the force obtained by the FFT self-consistent force calculation (see Section A1.4).

**Table A1.** Disc galaxy halo model parameters.

| Quantity | Symbol | Value | |
|---|---|---|---|
| | | Computational | Physical |
| Total mass | $M_{Halo}$ | 25000 | $1.24 \times 10^{11}\,M_\odot$ |
| No. particles | $N_{Halo}$ | 24953 | — |
| RMS radius | $\sqrt{< R_{Halo}^2 >}$ | 2.48 | 7.94 kpc |
| Moment of inertia | $I_{xx}$ | 1.46 | 4.67 kpc |
| | $I_{yy}$ | 1.45 | 4.64 kpc |
| | $I_{zz}$ | 1.38 | 4.42 kpc |
| Velocity dispersion | $\sigma_{Halo}$ | 0.136 | 220 km s$^{-1}$ |
| Vel. dispersion tensor | $\sigma_{xx}$ | 0.0781 | 126 km s$^{-1}$ |
| | $\sigma_{yy}$ | 0.0779 | 126 km s$^{-1}$ |
| | $\sigma_{zz}$ | 0.0804 | 130 km s$^{-1}$ |

This procedure is carried out by increasing $\Phi_{exp}$ from zero to its maximum magnitude over four crossing times with a King model consisting of approximately 25 000 particles. The final mass of the disc is 2/5 that of the halo. The halo with the full disc force imposed is allowed to relax for an additional two crossing times. The diagonal components of the moment of inertia tensor of the King model decreased by about 20 per cent along the axes coincident with the disc and by approximately 25 per cent in the normal direction as the disc potential was imposed. The rms velocity of the halo increased by 33 per cent. The imposition of the disc introduced no overall coherent streaming motion, although the velocity dispersion tensor naturally became anisotropic. See Table A1 for a list of halo parameters.

### *A1.3 Three-dimensional disc construction*

Since an exponential surface density disc and surrounding halo are desired, the simple distribution function formulation is not available for creating the disc galaxy. Instead, the gross observed characteristics of disc galaxies are used as a guide and a configuration is built which changes little over the collision time-scales. Stars are placed in circular orbits and given the random in-plane velocity dispersion needed to ensure disc stability (Toomre 1964). The structure of the disc in the vertical direction is less well known (see e.g., Bahcall & Soniera 1980; Gilmore, Wyse & Kuijken 1989). It is assumed that the self-gravity of the disc is the dominant contributor to the $z$-component of the local force field in the disc, and the first moment of the Vlasov equation and Poisson's equation are

$$\frac{\partial\rho(r,z)}{\partial z} + \frac{\rho(r,z)}{\sigma_z^2(r)}\frac{\partial\Phi(r,z)}{\partial z} = 0, \qquad \text{(A3)}$$

and

$$\frac{\partial^2\Phi(r,z)}{\partial z^2} = 4\pi G\rho(r,z), \qquad \text{(A4)}$$

where $\Phi$ is the gravitational potential, $\rho$ is the mass density, and $\sigma_z$ is the velocity dispersion in the $z$ direction. Derivatives involving $\Phi$ are eliminated from the two equations to get

$$\frac{\partial^2}{\partial z^2}\ln\rho(r,z) = -\frac{4\pi G\rho(r,z)}{\sigma_z^2(r)}. \qquad \text{(A5)}$$

This equation has the well-known solution (e.g., see Spitzer 1978)

$$\rho(r,z) = \rho(r,0)\ \mathrm{sech}^2(z/H), \tag{A6}$$

where

$$H \equiv \left(\frac{\sigma_z^2(r)}{2\pi G\,\rho(r,0)}\right)^{1/2}. \tag{A7}$$

This isothermal distribution means that at any given radius the velocity dispersion in the direction perpendicular to the disc (the $z$ direction) does not depend on $z$. Combining this with the exponential surface density

$$\Sigma(r) = \Sigma_0 \exp\left(-\frac{r}{R_d}\right) \tag{A8}$$

yields the total density

$$\rho(r,z) = \frac{M_{exp}}{4\pi H R_d^2} \exp\left(-\frac{r}{R_d}\right) \mathrm{sech}^2\left(\frac{z}{H}\right), \tag{A9}$$

where $M_{exp}$ is the formal total mass of the infinite exponential disc ($= 2\pi\Sigma_0 R_d^2$). In the above it is implicitly assumed that $H$ is a constant. A value for $H$ is chosen, which sets the $z$ velocity dispersion at any given radius.

In order to assign velocities the force law in the combined disc/halo potential is needed. The force in the disc plane is extracted numerically from the PM program and then fitted with a polynomial. This force law permits calculation of the circular velocity profile, $v_c$, the circular angular frequency, $\Omega(r)$, the epicycle frequency for small radial oscillations, $\kappa$, and Toomre's stability criterion, $Q$:

$$v_c(r) = \sqrt{r\,F(r)}, \tag{A10}$$

$$\Omega(r) = \sqrt{\frac{F(r)}{r}}, \tag{A11}$$

$$\kappa^2(r) = \left(r\frac{d\Omega^2}{dr} + 4\Omega^2\right), \tag{A12}$$

$$Q = \frac{\sigma_r(r)\,\kappa(r)}{3.36\,G\,\Sigma(r)}. \tag{A13}$$

A global value of $Q$=1.5 was chosen, which determined the radial velocity dispersion, $\sigma_r(r)$.

A rejection method is employed, similar to the one described in Press et al. (1986, p. 203), to populate the disc with particles. The spatial surface density in the disc plane is $\Sigma(r) = \Sigma_0 \exp(-r/R_d)$ and the total mass is $M_{exp} = 2\pi \int_0^\infty \Sigma(r)\,r\,dr = 2\pi\,\Sigma_0\,R_d^2$. So

$$\frac{2\pi \int_0^\infty \Sigma\, r\, dr}{2\pi\,\Sigma_0\,R_d^2} = \frac{\int_0^\infty \exp(-r/R_d)\,r\,dr}{R_{d^2}} = 1 \tag{A14}$$

We identify the probability distribution, $P(r)$, as

$$P(r) \equiv \frac{r\exp(-r/R_d)}{R_d^2}. \tag{A15}$$

Radii, $r$, are randomly picked in the range [0:$R_{max}$], where $R_{max}$ is some chosen cut-off radius, to obtain an associated value of $P(r)$. A second random number is chosen in the range [0:$P_{max}$], where $P_{max}$ is the maximum value of $P(r)$ ($P_{max} = \exp(-1)/R_d$). If the second random number is less than $P(r)$, a particle is placed at that radius and at a randomly chosen azimuth. If the second random number is greater than $P(r)$, that radius is rejected and the procedure is repeated. A similar method is used to distribute particles in the $z$-direction with the desired $\mathrm{sech}^2(z)$ profile.

**Table A2.** Stellar disc model parameters.

| Quantity | Symbol | Value | |
|---|---|---|---|
| | | Computational | Physical |
| Total mass | $M_{disc}$ | 9079 | $4.50 \times 10^{10}\,M_\odot$ |
| No. particles | $N_{disc}$ | 25000 | — |
| RMS radius | $\sqrt{< R_{disc}^2 >}$ | 2.53 | 8.10 kpc |
| RMS thickness | $I_{zz}$ | 0.196 | 627 pc |
| Avg. rotation vel. | $< v_\phi >$ | 0.131 | 217 km s$^{-1}$ |
| Vel. disp. tensor | $\sigma_{rr}$ | 0.0242 | 39.1 km s$^{-1}$ |
| | $\sigma_{\phi\phi}$ | 0.0395 | 63.8 km s$^{-1}$ |
| | $\sigma_{zz}$ | 0.0235 | 38.0 km s$^{-1}$ |
| Radial scale length | $R_d$ | 1.25 | 4 kpc |
| Radial cutoff | $R_{cut}$ | 5.5 | 17.6 kpc |
| Vertical scale height | $H$ | 0.25 | 800 pc |
| Toomre $Q$ | $Q$ | 1.5 | 1.5 |
| Cent. surface density | $\Sigma_0$ | 1016.5 | 492 $M_\odot$ pc$^{-2}$ |

For a given $r$ and a specified value of $Q$, the circular speed and radial velocity dispersion are calculated. For consistency we are led to the relationship (see Binney & Tremaine 1987)

$$\frac{\sigma_\phi^2}{\sigma_r^2} = \frac{\kappa^2}{4\Omega^2}, \tag{A16}$$

where $\sigma_\phi$ is the azimuthal velocity dispersion. The specific radial velocity for a particle is chosen from a Gaussian distribution with the desired dispersion using the rejection method. An additional azimuthal velocity is chosen in the same manner and added to the circular velocity. Given a value of the vertical scale height, $H$, a $z$ velocity is likewise chosen from a Gaussian.

This method gives a disc which is approximately initially in a steady state. Possible problems arise from the thin disc approximations and from the fact that the azimuthal velocities are not corrected for the presence of random motions in the disc plane. (This latter effect decreases the azimuthal velocity needed to remain in steady state. In the limit of very large random motions, the average azimuthal velocity at any radius tends toward zero.) Due to their small magnitudes these corrections are not of major concern for the collision experiments. The parameters used for the disc model are given in Table A2.

### *A1.4 Disc gas distribution*

The gas density distribution in the disc follows the same form as the stellar distribution. The gas is supported in the radial direction primarily by rotation and we seek the pressure, $P$, necessary to support the gas to a specified scale height perpendicular to the plane of the disc. Use is made of the equation of hydrostatic equilibrium

$$\frac{\partial P(r,z)}{\partial z} = -\rho_{gas}\frac{\partial \Phi(r,z)}{\partial z}, \tag{A17}$$

and equation (A3),

$$\frac{\partial \Phi(r,z)}{\partial z} = -\frac{\sigma_z^2}{\rho_{total}}\frac{\partial \rho_{total}}{\partial z}, \tag{A18}$$

where $\rho_{gas}$ is the gas density and $\rho_{total}$ is the total mass density (gas plus stars). We define $\eta$ as the ratio of gas density, $\rho_{gas}$, to total density, $\rho_{total}$,

$$\eta \equiv \frac{\rho_{gas}}{\rho_{total}} = \eta(r) \quad \text{at} \quad \text{most.} \tag{A19}$$

**Table A3.** Gas disc model parameters.

| Quantity | Symbol | Value | |
|---|---|---|---|
| | | Computational | Physical |
| Total mass | $M_{gas}$ | 894 | $4.43 \times 10^9\ M_\odot$ |
| No. particles | $N_{sph}$ | 22506 | — |
| Initial particle separation | $dl$ | 0.159 | 509 pc |
| smoothing length | $h$ | 0.223 | 714 pc |
| central density | $\rho(0,0)$ | 203.3 | $1.25\, m_H$ cm$^{-3}$ |
| central sound speed | $c(0)$ | 0.0323 | 52.2 km s$^{-1}$ |
| central temperature | $T(0)$ | | $3.25 \times 10^5 (\frac{m}{m_H})$ K |

Combining equations (A16) and (A17), we have

$$\frac{\partial P}{\partial z} = \sigma_z^2 \eta \frac{\partial \rho_{total}}{\partial z}, \tag{A20}$$

which has the solution

$$P = [\sigma_z^2 \eta]\, \rho_{total} = \sigma_z^2\, \rho_{gas}. \tag{A21}$$

Comparing this with the isothermal equation of state, $P = \rho c^2$, we identify $c^2 = \sigma_z^2$ so that the stars (in the $z$-direction) have the same 'temperature' as the gas. With the gas scale height set equal to the stars' scale height the gas temperature falls off exponentially with radius. An alternative prescription has been used by Hernquist & Weil, in which the temperature is spatially constant.

Table A3 contains computational parameters used for the gas disc.

This paper has been produced using the Royal Astronomical Society/Blackwell Science LaTeX style file.